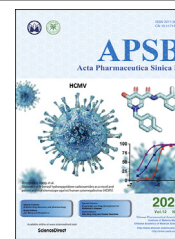




Chinese Pharmaceutical Association
Institute of Materia Medica, Chinese Academy of Medical Sciences

Acta Pharmaceutica Sinica B

www.elsevier.com/locate/apsb
www.sciencedirect.com



ORIGINAL ARTICLE

Characterization of a novel bispecific antibody targeting tissue factor-positive tumors with T cell engagement

Zhidi Pan^a, Jie Chen^a, Xiaodong Xiao^{b,c}, Yueqing Xie^b, Hua Jiang^{b,c},
Baohong Zhang^a, Huili Lu^a, Yunsheng Yuan^a, Lei Han^c,
Yuexian Zhou^a, Huifang Zong^a, Lei Wang^a, Rui Sun^a,
Jianwei Zhu^{a,b,c,*}

^aEngineering Research Center of Cell & Therapeutic Antibody, MOE, School of Pharmacy, Shanghai Jiao Tong University, Shanghai 200240, China

^bJecho Laboratories, Inc., Frederick, MD 21704, USA

^cJecho Biopharmaceuticals Co., Ltd., Tianjin 300467, China

Received 9 July 2021; received in revised form 1 October 2021; accepted 14 October 2021

KEY WORDS

T cell engaging bispecific antibody;
Immunotherapy;
Tissue factor;
Solid tumor;
Pancreatic cancer;
Lung cancer;
PD-1 antibody

Abstract T cell engaging bispecific antibody (TCB) is an effective immunotherapy for cancer treatment. Through co-targeting CD3 and tumor-associated antigen (TAA), TCB can redirect CD3⁺ T cells to eliminate tumor cells regardless of the specificity of T cell receptor. Tissue factor (TF) is a TAA that involved in tumor progression. Here, we designed and characterized a novel TCB targeting TF (TF-TCB) for the treatment of TF-positive tumors. *In vitro*, robust T cell activation, tumor cell lysis and T cell proliferation were induced by TF-TCB. The tumor cell lysis activity was dependent upon both CD3 and TF binding moieties of the TF-TCB, and was related to TF expression level of tumor cells. *In vivo*, in both tumor cell/human peripheral blood mononuclear cells (PBMC) co-grafting model and established tumor models with poor T cell infiltration, tumor growth was strongly inhibited by TF-TCB. T cell infiltration into tumors was induced during the treatment. Furthermore, efficacy of TF-TCB was further improved by

Abbreviations: AUC_{0–t}, area under the curve from time zero to the last quantifiable concentration; CL, clearance; C_{max}, the maximum plasma concentration; DSC, differential scanning calorimetry; FVII, factor VII; H-scores, Histo scores; i.p., intraperitoneally; i.v., intravenously; IHC, immunohistochemistry; MFI, mean fluorescence intensity; PBMC, human peripheral blood mononuclear cells; PEI, polyethyleneimine; PK, pharmacokinetics; s.c., subcutaneously; SE-HPLC, size exclusion-high performance liquid chromatography; *t*_{1/2}, half-life; TAA, tumor-associated antigen; TCB, T cell engaging bispecific antibody; TF, Tissue factor; UPLC–QTOF-MS, ultra-performance liquid chromatography coupled with quadrupole time-of-flight mass spectrometry; V_{d,ss}, steady-state volume of distribution.

*Corresponding author.

E-mail address: jjianweiz@sjtu.edu.cn (Jianwei Zhu).

Peer review under responsibility of Chinese Pharmaceutical Association and Institute of Materia Medica, Chinese Academy of Medical Sciences.

<https://doi.org/10.1016/j.apsb.2021.10.028>

2211-3835 © 2022 Chinese Pharmaceutical Association and Institute of Materia Medica, Chinese Academy of Medical Sciences. Production and hosting by Elsevier B.V. This is an open access article under the CC BY-NC-ND license (<http://creativecommons.org/licenses/by-nc-nd/4.0/>).



combination with immune checkpoint inhibitors. For the first time, our results validated the feasibility of using TF as a target for TCB and highlighted the potential for TF-TCB to demonstrate efficacy in solid tumor treatment.

© 2022 Chinese Pharmaceutical Association and Institute of Materia Medica, Chinese Academy of Medical Sciences. Production and hosting by Elsevier B.V. This is an open access article under the CC BY-NC-ND license (<http://creativecommons.org/licenses/by-nc-nd/4.0/>).

1. Introduction

T cell engaging bispecific antibody (TCB) is an essential component in T cell-based immunotherapy for cancer treatment. Through co-targeting CD3 on T cells and tumor-associated antigen (TAA) on tumor cells, TCB can recruit T cells to kill tumor cells independent of epitope specificity of T cell receptor and bypassing major histocompatibility complex restriction¹. Almost all CD3⁺ T cells, including CD8⁺ T cells, CD4⁺ T cells, regulatory T cells can act as effector cells to eliminate tumor cells^{2–4}. Therefore, unlike immune-checkpoint inhibitors, TCB can be efficacious even for tumors with a low neoantigen burden and T cell infiltration^{4–6}. The therapeutic potential of TCB was exemplified by blinatumomab, a TCB approved by the US Food and Drug Administration and dozens of TCBs in the clinical trials for the treatment of hematological malignancies^{1,7}.

In solid tumor, only a few TCBs (cibisatamab and tebentafusp) have shown early signs of anti-tumor activity in the clinical trials^{5,8}. More efficacious TCBs targeting new antigens, new epitopes or using new molecular formats and/or combination strategies are highly desirable to enrich this pipeline.

Tissue factor (TF), also known as CD142, is a 47 kDa transmembrane glycoprotein belonging to class II cytokine receptors superfamily⁹. It is highly expressed in a variety of cancers, such as pancreatic cancer, hepatocellular cancer, colorectal cancer, breast cancer, prostate cancer and bladder cancer. High TF expression level is frequently associated with poor prognosis^{10–16}. Under normal physiologic conditions, TF expression is restricted to the cells of the subendothelial vessel wall, like fibroblasts, and body surfaces, like epithelial cells^{17,18}. Upon binding to its ligand factor VII (FVII), TF converts it into activated isoform (FVIIa). The TF:FVIIa complex is involved in tumor growth, angiogenesis and metastasis through its procoagulant activity and ability to induce intracellular signaling¹⁹.

TF represents an appealing target for the treatment of solid tumors. Versteeg et al.²⁰ reported that direct blockage of TF:FVIIa mediated intracellular signaling by TF antibody 10H10 effectively inhibited tumor growth. Tisotumab Vedotin, an antibody–drug conjugate targeting TF showed potent TF dependent cytotoxicity *in vitro* and *in vivo*²¹. In all patients-derived xenograft models, complete tumor regression was achieved, even in tumors with only 25% to 50% tumor cells expressing TF²¹. In two phase I/II clinical trials, Tisotumab Vedotin showed manageable safety profile and encouraging antitumor activity (15.6% objective response was achieved among patients with relapsed, advanced, or metastatic cancer, 22% objective response was achieved among patients with recurrent or metastatic cervical cancer)^{22,23}.

After confirming TF expression profile and screening primary activities, we constructed a novel TCB targeting TF (TF-TCB) adopting the IgG-[L]-scFv structure. TF-TCB was highly potent

against a panel of tumor cell lines expressing TF *in vitro*. *In vivo*, it inhibited tumor growth in both tumor cell/human peripheral blood mononuclear cells (PBMC) co-grafting model and established tumor models with intravenous transfer of PBMC. The CD3 and TF labeling of the stripped tumors demonstrated TF-TCB-mediated T cell infiltration and TF⁺ tumor cells cleaning up as mechanism of tumor inhibition. Furthermore, combining TF-TCB with immune checkpoint inhibitors showed synergistic effect.

2. Materials and methods

2.1. Cells

HEK 293F cells were purchased from Invitrogen (Carlsbad, CA, USA). Jurkat, AsPC-1, PANC-1, MDA-MB-231, SKOV-3, NCI-H292 and CT-26 cells were obtained from Cell Bank of the Chinese Academy of Sciences (Shanghai, China), where they were authenticated by short tandem repeat profiling and tested mycoplasma free. All cell lines were cultured under supplier-recommended conditions and used within 2 months after resuscitation. PBMC used for the reconstruction of human immune system in NOG mice and CD3⁺ T cells used for the T cell activation test were bought from AllCells (Shanghai, China). PBMC used in other experiments were isolated from leukocyte concentrate (AllCells) using Ficoll-Paque PLUS (GE Healthcare Life Sciences, Uppsala, Sweden).

2.2. Antibody production and characterization

Genes of TF-TCB, TF-011 and CD22-TCB were synthesized by General Biosystems (Hefei, China), and were subcloned into a mammalian expression vector pCDNA 3.4 (Invitrogen) through homologous recombination. Plasmids with antibody genes were then extracted using Endo-Free Plasmid Maxi Kit (Omega Bio-Tek, Norcross, GA, USA) following manufacturer's instructions and transiently transfected into HEK 293F cells²⁴. The transfection process is as follows: HEK 293F cells were seeded at 0.6×10^6 – 0.7×10^6 cells/mL. Twenty-four hours later, cells were counted and diluted to 1×10^6 cells/mL. Plasmids ($0.6 \mu\text{g}/10^6$ cells) were diluted with FreeStyle 293 Expression Medium (Gibco, Carlsbad, CA, USA) to a concentration of 40 $\mu\text{g}/\text{mL}$ and mixed with 25-kDa polyethyleneimine (PEI, Polysciences, Warrington, PA, USA) (DNA:PEI = 1:4, w/w). After incubation for 10–15 min at room temperature, the mixture was added to the cell culture. The culture supernatant was harvested 4–6 days post transfection and antibodies were purified by protein A affinity chromatography (GE Healthcare Life Sciences) as previously described²⁵.

The antibody purity was assessed by SDS-PAGE and size exclusion-high performance liquid chromatography (SE-HPLC).

The SE-HPLC was performed on an Agilent HPLC system using a TSKgel G3000SW_{XL} HPLC Column (7.8 mm × 300 mm) (Agilent Technologies, Santa Clara, CA, USA). The molecular weight of intact and deglycosylated TF-TCB were determined as follows: TF-TCB was buffer-exchanged into 50 mmol/L ammonium bicarbonate (pH 8.0) and concentrated to 2 mg/mL by ultrafiltration; half of the sample was get out for intact molecular weight measurement; the other half was incubated with PNGase F (Yeasen Biotech, Shanghai, China) at 37 °C for 24 h to remove the N-glycan; the molecular weight was determined using ultra-performance liquid chromatography coupled with quadrupole time-of-flight mass spectrometry (UPLC-QTOF-MS; Waters, Etten-Leur, Netherlands).

2.3. Stability analysis

The conformational stability of TF-TCB was measured by differential scanning calorimetry (DSC) using NanoDSC (TA instruments, New Castle, DE, USA). TF-TCB and control antibody TF-011 (in PBS buffer) were heated from 20 °C up to 95 °C at a rate of 1 °C/min. The data were analyzed using NanoAnalyze software.

The storage stability of TF-TCB (0.5 mg/mL in PBS buffer) was evaluated by SE-HPLC and cation exchange chromatography analysis after 1, 2, 3 or 4 weeks of storage at 4, 25 or 40 °C. The cation exchange chromatography was performed on an Agilent HPLC system using a ProPac WCX-10 HPLC column (4 mm × 250 mm; Thermo Scientific, Waltham, MA, USA).

2.4. Binding analysis

2.4.1. Biacore

The affinities and kinetics of the TF-TCB binding to CD3D × CD3E and TF antigen were evaluated by surface plasmon resonance (Biacore 8K, GE Healthcare Life Sciences). TF-011, an anti-TF antibody sharing the same TF binding moieties with the TF-TCB, was used as control²¹. CD3D × CD3E heterodimer (Sino Biological, Beijing, China) or the TF antigen (Peprotech, Rocky Hill, NJ, USA) was immobilized to CM5 chip surface using routine 1-ethyl-3-(3-dimethylaminopropyl) carbodiimide/*N*-hydroxysuccinimide amine coupling protocols. The immobilization buffer was 10 mmol/L sodium acetate (pH 4.5, GE Healthcare Life Sciences). Surface densities after immobilization ranged from 50 to 100 RU. Two-fold serial dilutions of antibodies (TF-TCB or TF-011) ranging from 0.318 to 162.8 nmol/L in HBS-EP running buffer (GE Healthcare Life Sciences) were used to analyze binding. Running buffer alone was used as a zero reference. The antibodies were injected for 200 s followed by 180 s of dissociation time. Surface was regenerated by 0.1 mol/L glycine (pH 1.5) for 30 s. Data were analyzed using a 1:1 Langmuir binding model to calculate the kinetics and binding constants.

2.4.2. Cellular binding

The binding ability of TF-TCB to cell surface CD3 and TF was measured by flow cytometry. MDA-MB-231 cells (2×10^5 cells/well) or Jurkat cells (2×10^5 cells/well) were placed into 96-well U bottom-plate (Corning, Corning, NY, USA) after resuspension in FACS buffer (2% fetal bovine serum in PBS buffer). Test antibodies were serially diluted 1:3 in FACS buffer and added to the cells in a total volume of 100 μL. After incubation on ice for 30 min, cells were washed 3 times with FACS buffer and resuspended in 100 μL 1:200 goat anti-human IgG (H + L) secondary antibody (FITC-labeled, Invitrogen) in FACS buffer. Cells were

incubated for another 30 min on ice. After washing 3 times with FACS buffer, mean fluorescence intensity (MFI) of cells was analyzed on FACSCalibur (Beckman Coulter, Fullerton, CA, USA). The binding EC₅₀ value based on MFI was calculated in GraphPad Prism using non-linear regression analysis for single site binding²⁶.

2.5. Conjugates formation test

CD3⁺ Jurkat cells and TF⁺ AsPC-1 cells were labeled with PKH26 (Sigma—Aldrich, St. Louis, MO, USA) and CFSE (Invitrogen) respectively under manufacturer's guidelines. The two labeled cell lines were resuspended in FACS buffer and mixed at a ratio of 1:1. TF-TCB (50 ng/mL), TF-011 (50 ng/mL) or PBS was added to the mixture in a total volume of 100 μL. After incubation at 37 °C, 5% CO₂ for 30 min, the mixtures were analyzed on FACSCalibur. Crosslinking of CD3⁺ Jurkat cells and TF⁺ AsPC-1 cells by TF-TCB or TF-011 was evaluated through the appearance of PKH26⁺/CFSE⁺ cell—cell conjugates.

2.6. T cell activation and cytokine release determination

AsPC-1 cells (1.2×10^4 cells/well) or culture medium were added in flat-bottom 96-well plate (Corning). After 24 h of adherent culture, effector cells (PBMC or CD3⁺ T cells; E:T, 10:1) and TF-TCB (or TF-011) were added into the well and co-incubated for 20 h. Then, effector cells and supernatant were collected. Effector cells were washed 1 time using FACS buffer and stained with FITC-labeled anti-CD8 (Sino Biological), PE-labeled anti-CD4 (Sino Biological) and APC-labeled anti-CD69 antibodies (BD Biosciences, San Jose, CA, USA) under manufacturer's instructions. After washing 3 times with FACS buffer, effector cells were analyzed on FACSCalibur. The percentages of CD69⁺ cells within CD4⁺ and CD8⁺ T cell populations was calculated. Cytokines (IFNγ and IL-2) released into the supernatant were measured using IFNγ immunoassay kit (R&D Systems, Minneapolis, MN, USA) and IL-2 immunoassay kit (R&D Systems).

2.7. T cell proliferation assay

AsPC-1 cells were seeded in flat-bottom 96-well plate and cultured for 24 h. CD3⁺ T cells were isolated from PBMC by human CD3 isolation kit (Invitrogen) and were labeled with CFSE. Labeled T cells were added into AsPC-1 cell culture (E:T, 10:1) in the presence of TF-TCB (1 μg/mL). Labeled T cells alone, labeled T cells incubated with AsPC-1 cells or TF-TCB were used as controls. Ninety-six hours later, the T cells were harvested and analyzed for fluorescence on FACSCalibur.

2.8. Measurement of relative antigen expression on tumor cells and T cells

For measurement of TF expression, tumor cells (1×10^5 cells/well) were placed into 96-well U bottom-plate after resuspension in FACS buffer and stained with or without FITC-labeled anti-TF antibody (Sino Biological) under manufacturer's instructions. Relative TF expression was represented by comparing cell fluorescence intensity of anti-TF antibody group with blank control group.

For measurement of PD-L1 expression on tumor cells, FITC-labeled anti-TF antibody was replaced by APC-labeled anti-PD-L1 antibody (Sino Biological).

For PD-1 staining of CD3⁺ T cells, PBMC were harvested after 36 h of incubation with or without TF-TCB in the presence or absence of tumor cells, and stained with FITC-labeled anti-CD3 antibody (Sino Biological) and APC-labeled anti-PD-1 antibody (Sino Biological) under manufacturer's instructions. PD-1 expression on CD3⁺ T cells was then analyzed on FACSCalibur.

For PD-L1 staining of AsPC-1 and NCI-H292 cells, AsPC-1 and NCI-H292 cells were harvested after 36 h of incubation with or without TF-TCB in the presence or absence of PBMC, and stained with FITC-labeled anti-TF antibody (Sino Biological) and APC-labeled anti-PD-L1 antibody (Sino Biological) under manufacturer's instructions. PD-L1 expression on TF⁺ tumor cells was then analyzed on FACSCalibur.

2.9. *In vitro* tumor cell lysis assays

In vitro tumor cell lysis was assayed by CytoTox 96 Non-Radioactive Cytotoxicity Assay Kit (Promega, Madison, WI, USA) as described previously²⁵. Briefly, tumor cells were seeded in a flat-bottom 96-well plate. After 24 h of adherent culture, test antibodies were added and incubated for 30 min at 37 °C. Then PBMC were added into the culture. After additional 24 or 36 h of incubation, the lactate dehydrogenase activity in the supernatant representing cell lysis was measured. The percentage of tumor cell lysis was calculated as Eq. (1):

$$\text{Tumor cell lysis (\%)} = \frac{(\text{Experimental lysis} - \text{Spontaneous PBMC lysis} - \text{Spontaneous tumor cell lysis}) / (\text{Maximum tumor cell lysis} - \text{Spontaneous tumor cell lysis}) \times 100}{(1)}$$

The tumor cell lysis EC₅₀ was calculated in GraphPad Prism software using non-linear regression analysis for log (inhibitor) vs. response-variable slope.

2.10. *In vivo* studies

All animal experiments were conducted in compliance with guidelines from Institutional Animal Care and Use Committee of the School of Pharmacy of Shanghai Jiao Tong University (Shanghai, China). Six-to eight-week-old mice at experiment initiation were purchased from Charles River Laboratories (Beijing, China).

2.10.1. Pharmacokinetics (PK) analysis

Male BALB/c mice were divided into two groups based on body weight ($n = 5/\text{group}$). TF-TCB and control antibody TF-011 were single-intravenously (i.v.) injected into mice at 5 mg/kg. Mice blood was then collected at the following time points: 0 (predose), 15 min, 6 h, 1, 2, 4, 7, 10, 15, 21 and 28 days. The antibody concentration in blood serum was quantified by ELISA. PK parameters were determined with a noncompartmental analysis model using PKsolver.

2.10.2. AsPC-1/PBMC co-grafting model

AsPC-1 cells (2×10^6 cells) and PBMC (2×10^6 cells, freshly isolated) were admixed in a total volume of 100 μL in RPMI 1640 medium (Gibco) and implanted subcutaneously (s.c.) into female NOD/SCID mice. NOD/SCID mice were then divided into five groups based on body weight ($n = 6/\text{group}$). Vehicle control (PBS), TF-011 (1 mg/kg) or TF-TCB (0.2, 1 or 5 mg/kg) was administered i.v. following the experimental schedule (Fig. 5A).

Mice weight and tumor dimensions (length and width) were recorded from Day 4 to study completion. Tumor volume was estimated using Eq. (2):

$$\text{Tumor volume (mm}^3\text{)} = (\text{Length} \times \text{Width} \times \text{Width})/2 \quad (2)$$

After mice were sacrificed, tumors were stripped, weighed, and photo recorded.

2.10.3. AsPC-1 xenograft model with intravenous transfer of PBMC

Female NOG mice were injected s.c. with AsPC-1 cells (2×10^6 cells) on Day 0, 9 days later, tumor dimensions were measured and tumor volume was estimated as above. Mice were divided into four groups (PBS/PBS group, PBS/Gemcitabine group, PBMC/PBS group and PBMC/TF-TCB group, $n = 6/\text{group}$) based on tumor volume. Gemcitabine was bought from Haosen (Jiangsu, China). On Day 10, 5×10^6 resuscitated PBMC were injected i.v. into mice of PBMC/PBS group and PBMC/TF-TCB group. Mice in other two groups were injected with PBS instead. On Day 11, mice in PBS/PBS group and PBS/Gemcitabine group were administrated with PBS and gemcitabine (100 mg/kg) intraperitoneally (i.p.) respectively, mice in PBMC/PBS group and PBMC/TF-TCB group were administrated with PBS and TF-TCB (5 mg/kg) i.v. respectively following the experimental schedule (Fig. 6A). Tumor dimensions were measured once per week till study completion and tumor volume was estimated as above. Graft-versus-host disease is a common phenomenon in this tumor model. Study was terminated when graft-versus-host disease was evident. After mice were sacrificed, tumors were stripped, weighed, and photo recorded.

On Day 24, 14 days after PBMC transfer, reconstruction of human immune system in NOG mice was evaluated. 100 μL blood of mice was collected and incubated with FITC labeled anti-human CD45⁺ antibody (Sino Biological) at room temperature for 30 min. Then the blood was added 2 mL red blood cell lysis buffer (Invitrogen) and incubated for another 10 min. Cells were washed 2 times using FACS buffer, and percentage of human CD45⁺ cells in mice peripheral blood was evaluated on FACSCalibur.

2.10.4. NCI-H292 xenograft model with intravenous transfer of PBMC

Female NOG mice were injected s.c. with NCI-H292 cells (3×10^6 cells) on Day 0. Three days later, 5×10^6 resuscitated PBMC were injected i.v. into mice. On Day 9, mice were divided into four groups based on tumor volume, and were administrated with PBS, nivolumab (10 mg/kg, i.p.), TF-TCB (5 mg/kg, i.v.) or combination of nivolumab (10 mg/kg, i.p.) and TF-TCB (5 mg/kg, i.v.) following the experimental schedule (Fig. 9A). Tumor dimensions were measured till study completion and tumor volume was estimated. After mice were sacrificed, tumors were stripped, weighed, and photo recorded. Fourteen days after PBMC grafting, reconstruction of human immune system in NOG mice was evaluated as mentioned above.

2.11. Immunohistochemistry (IHC) analysis

Stripped tumors were fixed in 4% paraformaldehyde (Servicebio, Wuhan, China) for 24 h, and embedded in paraffin. Tumor sections

(3 μm) were cut, followed by deparaffinization, heat antigen retrieval and endogenous peroxidase blocking of the tumor sections. Subsequently, the tumor sections were blocked with 3% bovine serum albumin in PBS for 30 min and incubated with anti-human CD3 rabbit antibody (Sino Biological), anti-human PD-L1 rabbit antibody (Cell Signaling Technology, Beverly, MA, USA) or anti-human TF rabbit antibody (Cell Signaling Technology) for overnight at 4 °C. Biotinylated goat anti-rabbit IgG (Servicebio) were then added and incubated for 50 min. Detection was conducted with DAB detection kit (Dako, Carpinteria, CA, USA) according to manufacturer's instructions. The tumor sections were counterstained with hematoxylin (Servicebio). Images were acquired using the OLYMPUS BX53 Microscope.

A multi-tumor tissue microarray and a multi-organ normal tissue microarray were bought from Bioitech (Xi'an, China) and stained with anti-TF antibody following the same protocol applied to tumor sections.

The tumor sections and tissue microarrays were evaluated for TF, CD3 or PD-L1 expression based on Histo scores (H-scores) and/or percentage of positive cells. Staining intensity (not colored, light brown, brown and tan were defined as 0, 1, 2 and 3) and percentages of stained cells of each staining intensity were recorded by a certified pathologist. The H-scores were calculated as Eq. (3):

$$\text{H-score} = 1 \times \text{percentage of cells staining at 1} + 2 \times \text{percentage of cells staining at 2} + 3 \times \text{percentage of cells staining at 3} \quad (3)$$

2.12. Statistical analysis

Data are shown as mean \pm standard deviation (SD) and statistical analysis was based on two-tailed heteroscedastic Student's *t*-test. The value of $P < 0.05$ was considered statistically significant

3. Result

3.1. Target determination

TAAAs are potential targets for anti-tumor treatment including cancer immunotherapy. Hundreds of TAAAs have been evaluated in cancer immunotherapy including CD19, BCMA, HER2, GPC3 and TF. A number of TCBs targeting different TAAAs were produced using BAPTS platform, a high throughput bispecific antibody platform^{25,28,55}, to validate whether TF was suitable to be a target of TCB. The TCBs were evaluated through T cell activation and tumor cell lysis activity, and TCB targeting TF revealed excellent anti-tumor activities (data not shown).

In parallel, TF expression in tumor and normal tissues was confirmed by IHC analysis performed upon a multi-tumor tissue microarray and a multi-organ normal tissue microarray. In tumor tissues, 92.1% lung squamous cell carcinomas, 55.2% invasive breast carcinomas of no specific type, 88.9% colonic adenocarcinomas, 85.7% prostate adenocarcinomas and 94.7% pancreatic ductal adenocarcinomas appeared positive (H-score ≥ 0) for TF. Except for invasive breast carcinomas, more than 40% carcinomas of other four types had high (H-score ≥ 100) TF expression level (Fig. 1A and Supporting Information Table S1). Correlation of TF expression intensity with pathological tumor grade or clinical stage was somewhat controversial^{13,29–31}. In our study, in all carcinoma types, no such correlation was observed (Supporting Information Tables S1 and S2). Although TF expression was found in several normal organs and limited cell types (such as epithelial cells, myocardial cells, neuroglial cells and ovarian granular cells), TF expression level in tumor tissues was higher than most normal tissues tested (Fig. 1B and Tables S1 and S3).

Based on expression differentiation in tumor vs. normal tissues, TF is a valuable target to be explored for TCB treatment, which was at certain degree validated by our initial anti-tumor experiments with

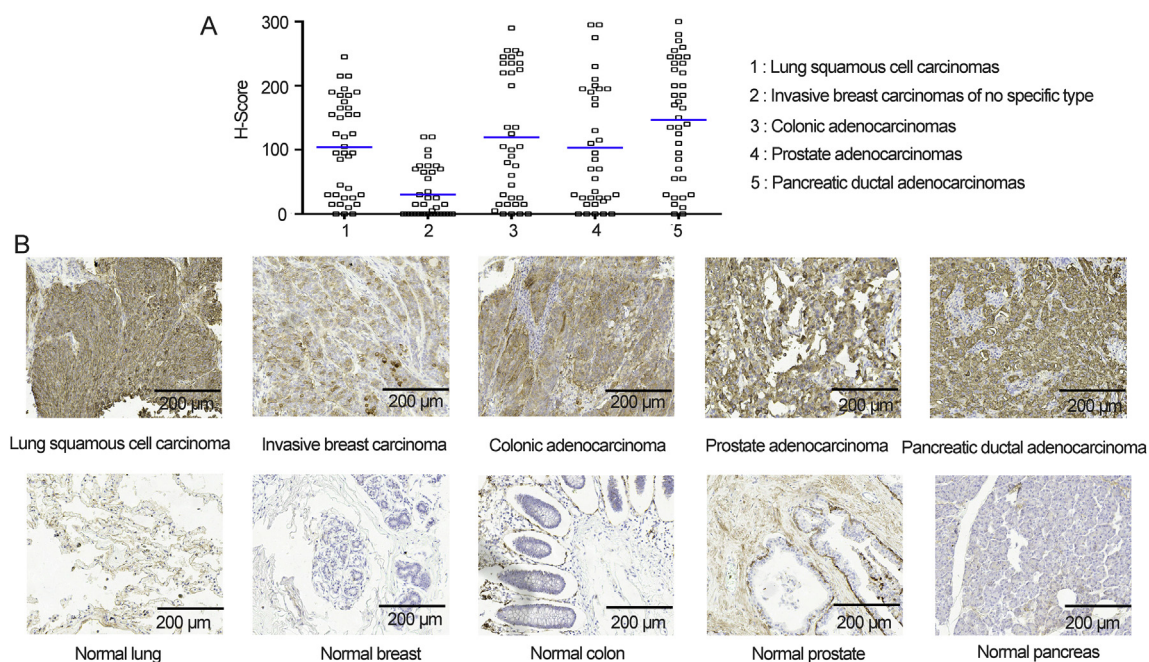


Figure 1 Tissue factor (TF) expression in tumor and normal tissues. (A) Histo scores (H-scores) describing TF cell surface expression across lung squamous cell carcinomas, invasive breast carcinomas of no specific type, colonic adenocarcinomas, prostate adenocarcinomas and pancreatic ductal adenocarcinomas. (B) Representative photomicrographs of TF staining of tumor and normal tissues. Scale bar is indicated in each panel.

TCB targeting TF. Therefore, these data encouraged us to investigate further on characterization of the TCB targeting TF-positive tumors.

3.2. Design and production of TF-TCB

The variable regions of TF-011 and a humanized version of OKT-3 were used as the binding moieties of TF-TCB^{21,32}. TF-011 is the antibody component of Tisotumab Vedotin. It could hinder TF:FVIIa induced intracellular signaling while having low interference with the pro-coagulant activity²¹. The preclinical and clinical evaluation of Tisotumab Vedotin illustrated the feasibility of targeting TF⁺ tumors using TF-011^{21,22,33}. Besides target binding moieties, format is important in most cases in developing a good therapeutic TCB. IgG-[L]-scFv is a normal IgG1 with an additional scFv linked to the C-terminus of each light chain. TCBs adopting this structure have shown better anti-tumor activity than that using normal IgG1, BITE or IgG-[H]-scFv structure (a normal IgG1 with an additional scFv linked to the C-terminus of each heavy chain) due to its dual bivalency and suitable interdomain space³⁴. Therefore, in our study, IgG-[L]-scFv format was adopted for TF-TCB (Fig. 2A). The linker of scFv to IgG was TSGGGGSGGGGSGGGGS. The IgG1 heavy and light chain was stabilized by introducing an interchain disulfide bond (G100C in the VL domain and G44C in the VH domain), so was the scFv³⁵. In order to abrogate the Fc-mediate non-specific activation of T cell, P329G LALA mutations were introduced to the Fc of TF-TCB. The TF-TCB therefore lacked complement-dependent cellular cytotoxicity and antibody-dependent cellular cytotoxicity activities with T cell being the only effector cell, as previously described³⁶. The nucleotide sequences of TF-TCB were shown in Supporting Information Table S4.

The TF-TCB was transiently expressed at around 10 mg/L. After one step of protein A affinity chromatography, purity of the TF-TCB in the eluate was higher than 95% by SE-HPLC and SDS-PAGE analysis (Fig. 2B and C). The molecular weight of intact TF-TCB and deglycosylated TF-TCB measured by UPLC-QTOF-MS were 200.952 kDa and 203.843 kDa respectively (Fig. 2D). The measured molecular weight of deglycosylated TF-TCB was consistent with its theoretical molecular weight (200.955 kDa) with error lower than 5 ppm (Fig. 2D). The measured molecular weight of intact TF-TCB was also in accordance with the non-reducing band of TF-TCB in the SDS-PAGE analysis (Fig. 2C and D). CD22-TCB employed the same structure of TF-TCB, while TF-011 was a normal IgG1 antibody. Their nucleotide sequences are shown in Table S4. CD22-TCB and TF-011 were expressed and purified in the same way as TF-TCB. SDS-PAGE analysis of CD22-TCB and TF-011 showed a purity over 90% (Supporting Information Fig. S1A and S1B). Nivolumab was expressed in a stably transfected CHO cell line constructed in our lab and purified through protein A affinity chromatography³⁷.

3.3. In vitro stability analysis of TF-TCB

The conformational stability of TF-TCB in PBS buffer was assessed by DSC. TF-TCB displayed three peak transitions, indicating 3 thermal unfolding events (Fig. 2E). Based on IgG structural framework of TF-TCB and DSC thermogram of TF-011, the three peaks (T_{m1} , T_{m2} and T_{m3}) of TF-TCB may be associated with the unfolding of its scFv domain, CH2 domain and CH3/Fab domains, respectively^{27,38,39}. And this could be further validated by comparing with the unfolding of CD3 scFv domain in future studies. Compared with TF-011, the introduction of two

CD3 scFv domains decreased the onset temperature of TF-TCB unfolding (Fig. 2E). In order to test the storage stability of TF-TCB, TF-TCB was stored at different temperature for different length of time. Charge variant profile of TF-TCB started to change after two-week storage at 25 °C and one-week storage at 40 °C (Supporting Information Fig. S2A). TF-TCB degradation represented by reduction of main peak area in SE-HPLC analysis started after one-week storage at 40 °C (Fig. S2B). However, there was no detectable change over 4-week storage at 4 °C, indicating the storage stability of TF-TCB at 4 °C (Fig. S2A and S2B).

3.4. Binding properties of TF-TCB

TF-TCB was a quadrivalent bispecific antibody with two CD3 and two TF binding moieties (Fig. 2A). The binding affinities of TF-TCB to CD3D × CD3E heterodimer and TF antigen measured by Biacore were 14.9 and 0.839 nmol/L respectively, comparable with other TCBs in clinical trials (Fig. 2F)¹.

For cell based binding analysis by flow cytometry, cell lines MDA-MB-231 (TF⁺) and Jurkat (CD3⁺) were used (Fig. 2G and H). TF-TCB dose-dependently bound to these two cell lines at EC₅₀ of 10.56 nmol/L (Jurkat) and 5.25 nmol/L (MDA-MB-231). TF-TCB shared the same TF binding moieties with TF-011. At both molecular and cellular level, their affinities to TF antigen were similar, suggesting that the binding affinity of a IgG1 was not interfered with by introduction of a scFv to the C terminus of light chain, which was in line with other TCBs using similar structure (Fig. 2G and H)^{34,40,41}.

3.5. Mechanism of action of TF-TCB

Upon simultaneous binding to TF⁺ tumor cells and CD3⁺ T cells, TF-TCB could cross-link these two groups of cells, induce T cell activation, cytokine release, tumor cell lysis and subsequently T cell proliferation. As shown in Fig. 3A, when TF⁺ AsPC-1 cells (CFSE labeled) and CD3⁺ Jurkat cells (PKH26 labeled) were incubated with TF-TCB, cross-linking of these two groups of cells were induced by TF-TCB with the appearance of CFSE⁺/PKH26⁺ cell-cell conjugates. While in the TF-011 or blank control group, there were almost no detectable CFSE⁺/PKH26⁺ cell-cell conjugates (Fig. 3A). To evaluate T cell activation mediated by TF-TCB, PBMC were incubated for 20 h with AsPC-1 cells and ten-fold serial dilutions of TF-TCB (or TF-011), and then collected for flow cytometry analysis. CD69 is an early sign of T cell activation. Compared with TF-011, dose-dependent activation of both CD4⁺ and CD8⁺ T cells was induced by TF-TCB as presented by percentage increase of CD69⁺ cells (Fig. 3B). TF-TCB showed similar activation of CD4⁺ and CD8⁺ T cells, with similar EC₅₀ (0.10 ng/mL for CD4⁺ T cells and 0.23 ng/mL for CD8⁺ T cells). Cytokine release (IL-2 and IFN γ), a hallmark of T cell activation upon tumor cell lysis was also induced by TF-TCB (Fig. 3C). In order to test the target-dependency of TF-TCB mediated T cell activation, CD3⁺ T cells were incubated with TF-TCB in the presence of target cells (AsPC-1 cells) or not for 20 h. It was shown that, only in the presence of AsPC-1 cells, CD4⁺ and CD8⁺ T cells could be activated by TF-TCB (Supporting Information Fig. S3). This suggested T cell activation induced by TF-TCB was target-dependent and two CD3 binding moieties of TF-TCB might not bind to the same T cell simultaneously. Tumor cell lysis was detected after 24 h (for MDA-MBA-231) or 36 h (for AsPC-1 and SKOV-3) of incubation of tumor cells with PBMC and test antibodies (Fig. 3D). Although TF-011 without

CD3 binding moiety could lysis TF⁺ tumor cells through antibody-dependent cellular cytotoxicity as previously described, TF-TCB had a much better activity, with much lower EC₅₀ and higher maximum percentage of tumor lysis (Fig. 3D)²¹. CD22-TCB had the same structure with TF-TCB, except that the TF binding moieties were replaced by CD22 binding moieties. Lysis of SKOV-3 cells was almost lost for CD22-TCB compared with TF-TCB, illustrating that the activity of TF-TCB was dependent on both its CD3 and TF binding moieties (Fig. 3D). In a CFSE cell division assay, apparent T cell proliferation was observed after incubation of T cells with both TF-TCB and target cells (AsPC-1) for 96 h, while co-incubation of T cells with TF-TCB or AsPC-1 cells alone was unable to promote T cell proliferation (Fig. 3E). T cell proliferation mediated by TF-TCB could support its serial elimination of tumor cells.

3.6. Association between TF expression level and tumor cell lysis activity of TF-TCB

To investigate the relationship between TF expression level and TF-TCB mediated tumor cell lysis activity, five tumor cell lines (CT-26, PANC-1, AsPC-1, SKOV-3 and MDA-MB-231) with different TF expression levels were used (Fig. 4A). After 36 h of incubation of these cells with PBMC (E:T, 15:1) and ten-fold serial dilutions of TF-TCB, tumor cell lysis was measured (Fig. 4B). TF-TCB could induce effective lysis of TF⁺ tumor cells with EC₅₀ ranging from 0.01 to 1.71 ng/mL (Fig. 4B). All TF⁺ tumor cells were killed with TF-TCB concentration higher than 100 ng/mL. For TF negative tumor cells, TF-TCB showed almost no lysis activity indicating the target dependence of cell lysis activity of TF-TCB (Fig. 4B). In general, tumor cell lysis

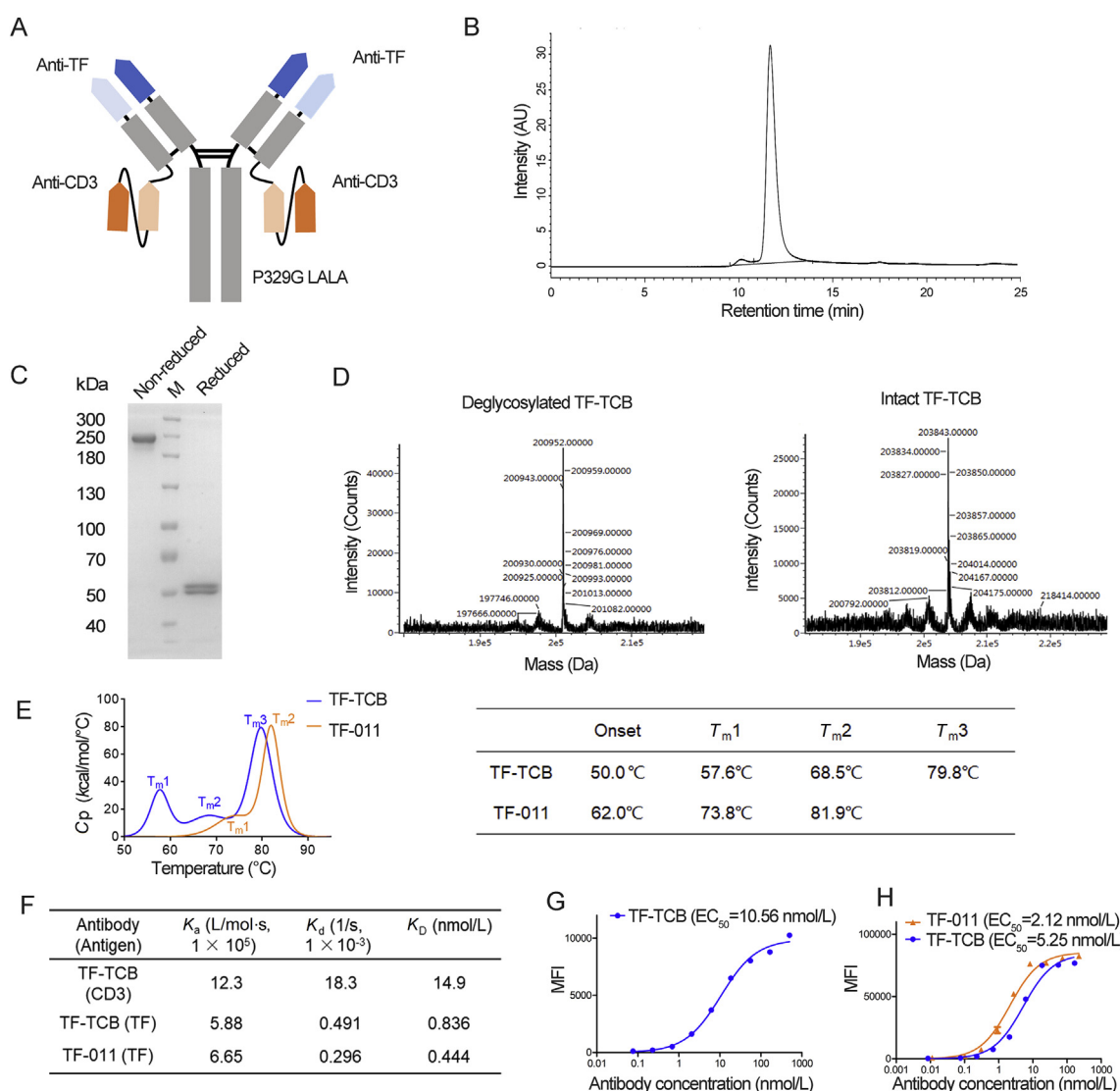


Figure 2 Structure and physico-chemical characterization of TF-TCB. (A) Schematic diagram of TF-TCB structure. (B) Size exclusion-high performance liquid chromatography (SE-HPLC) analysis of TF-TCB: the major peak (11.7 min, 96.7%) was the TF-TCB, the much smaller peak (10.1 min, 3.33%) might be the aggregates. (C) SDS-PAGE analysis of TF-TCB. (D) Ultra-performance liquid chromatography coupled with quadrupole time-of-flight mass spectrometry (UPLC-QTOF-MS) analysis of the molecular weight of intact and deglycosylated TF-TCB. (E) Differential scanning calorimetry (DSC) thermogram and corresponding T_m values of TF-TCB and TF-011. (F) Binding kinetics and affinities of TF-TCB and TF-011, measured by Biacore. (G) Binding affinity of TF-TCB to CD3⁺ Jurkat cells. (H) Binding affinities of TF-TCB and TF-011 to TF⁺ MDA-MB-231 cells. MFI, mean fluorescence intensity of tested cells. Data are mean \pm SD, $n = 3$.

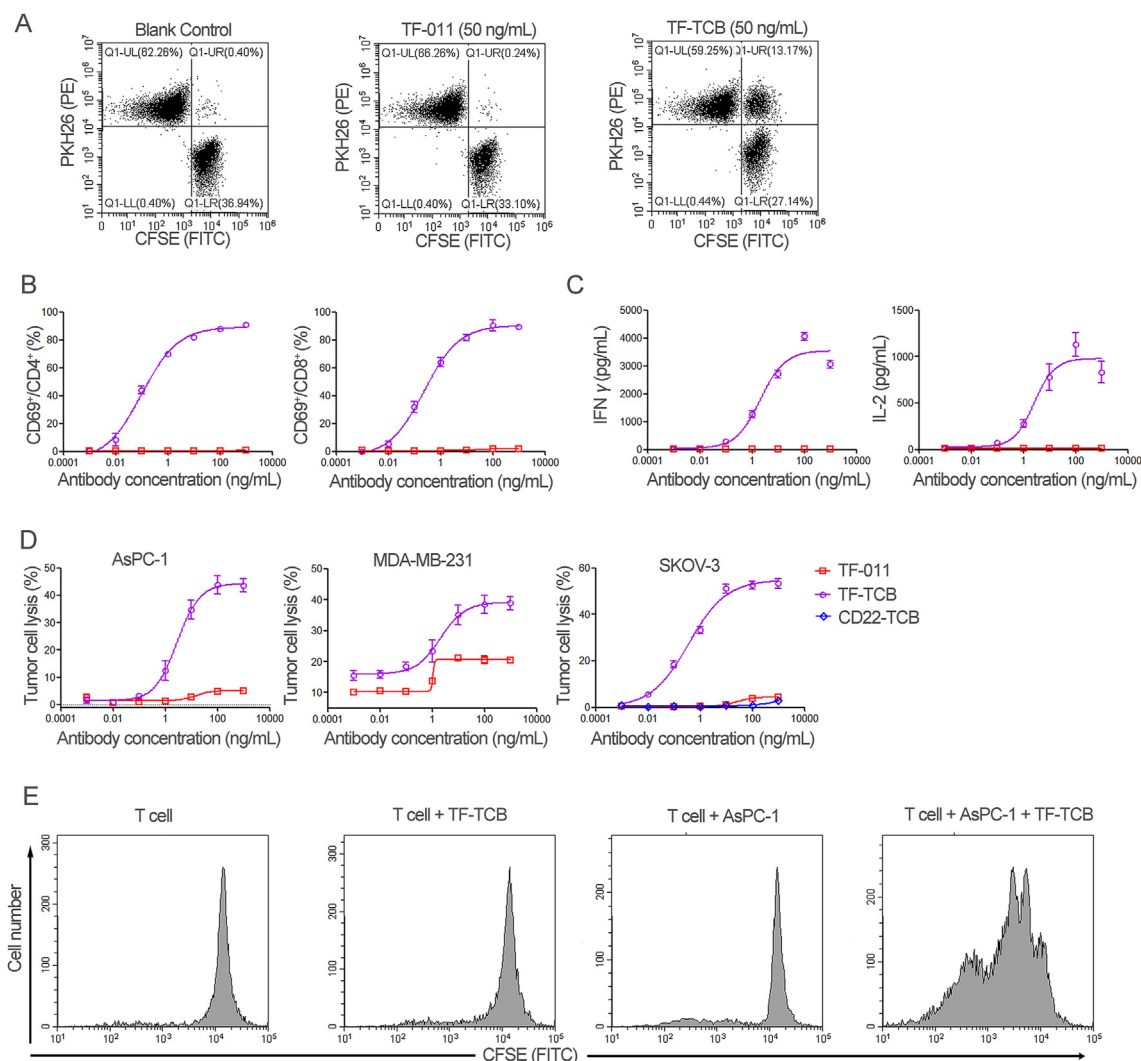


Figure 3 Mechanism of action of TF-TCB. (A) Cross-linking of CD3⁺ Jurkat cells and TF⁺ AsPC-1 cells by TF-TCB measured through flow cytometry. Jurkat cells were labeled with PKH26 (PE) and AsPC-1 cells were labeled with CFSE (FITC), the two cells were mixed at equal ratio in the presence of TF TCB (or TF-011) and incubated for 30 min. (B) and (C) T cell activation and cytokine release mediated by TF-TCB. T cell activation (B) was assessed by measuring percentage of CD69⁺ cells within CD4⁺ and CD8⁺ T cells after 20 h of incubation of human peripheral blood mononuclear cells (PBMC) with AsPC-1 cells (E:T, 10:1) and TF-TCB. IFN γ and IL-2 released into culture supernatant were also determined (C). TF-011 was used as control. (D) Percentage of tumor cell lysis detected after incubation of AsPC-1 (36 h), MDA-MB-231 (24 h) and SKOV-3 cells (36 h) with PBMC and TF-TCB. TF-011 and CD22-TCB were used as controls. (E) T cell proliferation evaluated through the decrease in CFSE labeling on T cells. Purified T cells were labeled with CFSE (FITC) and incubated with or without AsPC-1 cells, in the presence of TF-TCB or not for 96 h, and the CFSE labeling on T cells was evaluated by flow cytometry. Data are mean \pm SD, $n = 3$.

activity of TF-TCB was positively related to TF expression level on cell lines with higher potency for higher TF-expressing tumor cells. PANC-1 has lower TF expression level than AsPC-1 and SKOV-3, the stronger tumor cell lysis activity of TF-TCB towards PANC-1 was possibly due to differences in response to T cell cytotoxicity among the cell lines.

3.7. PK analysis of TF-TCB

The preliminary PK analysis of TF-TCB was performed in male BALB/c mice at a single dose of 5 mg/kg. TF-TCB showed a favorable PK profile with half-life ($t_{1/2}$) of \sim 8.25 days, suggesting its stability *in vivo* (Supporting Information Fig. S4A and S4B). The longer $t_{1/2}$ of TF-TCB compared with other bispecific

antibody formats (like BITE or TandAb) may be due to its Fc domain and relatively larger molecular weight^{34,40}. Compared with TF-011, TF-TCB had a shorter $t_{1/2}$, but similar area under the curve from time zero to the last quantifiable concentration ($AUC_{0-\infty}$, Fig. S4B). The smaller steady-state volume of distribution ($V_{d,ss}$) of TF-TCB suggested that it may have lower tissue penetration than TF-011 (Fig. S4B).

3.8. Tumor growth inhibition of TF-TCB in AsPC-1/PBMC co-grafting model

PBMC (2×10^6) and human metastatic pancreatic cancer cells AsPC-1 (2×10^6) were premixed and implanted s.c. in female NOD/SCID mice ($n = 6$ /group). Mice were then treated i.v. with

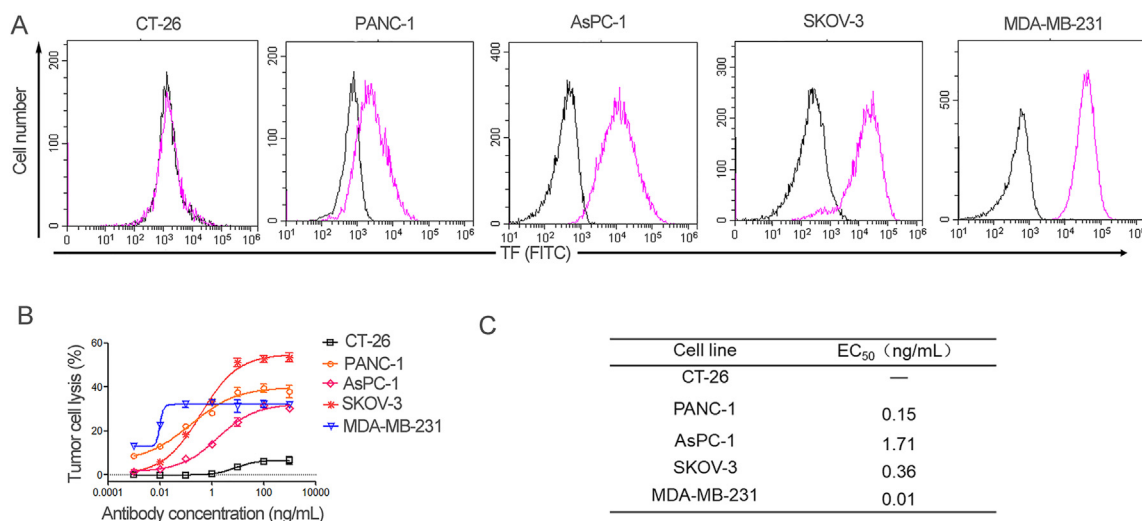


Figure 4 Correlation between TF expression level and tumor cell lysis activity of TF-TCB. (A) Relative TF expression on five tumor cell lines, detected by flow cytometry. Purple histogram, tumor cells stained with FITC-labeled anti-TF antibody; black histogram, Blank Control. (B) Percentage of tumor cell lysis detected after 36 h of incubation of target cells (CT-26, PANC-1, AsPC-1, SKOV-3 and MDA-MB-231) with PBMC (E:T, 15:1) and TF-TCB. (C) Cell lysis EC₅₀ values of the five tumor cells. Data are mean \pm SD, $n = 3$.

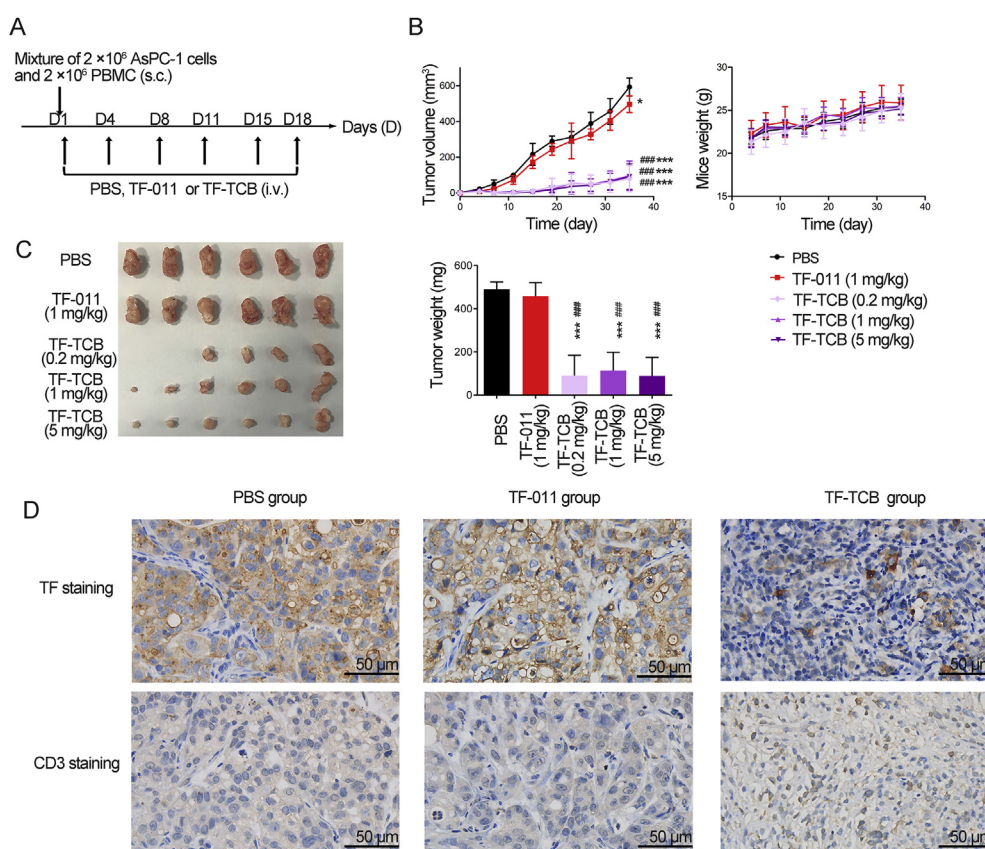


Figure 5 Inhibition of tumor growth by TF-TCB in AsPC-1/PBMC co-grafting model. (A) Schematic depiction of tumor inoculation and treatment protocol. Female NOD/SCID mice ($n = 6$ /group) were implanted subcutaneously (s.c.) with mixture of AsPC-1 cells (2×10^6) and PBMC (2×10^6) on Day 1, and administrated intravenously (i.v.) with PBS, TF-011 (1 mg/kg), or different doses of TF-TCB (0.2, 1 and 5 mg/kg) twice per week for a total of six doses. (B) Tumor volume and mice weight measured throughout the study. (C) Digital image and weight of the stripped tumors, two mice in the TF-TCB group (dose of 0.2 mg/kg) had no detected tumor when study completed. (D) Immunohistochemistry (IHC) analysis of tumors gained 6 days after first treatment. Tumors were stained for human TF and human CD3 (all brown) and were counterstained with hematoxylin (blue). Scale bar is indicated in each panel. Statistical analysis was based on two-tailed heteroscedastic *t*-test. * $P < 0.05$ and *** $P < 0.0001$ vs. PBS group, ### $P < 0.0001$ vs. TF-011 group. Data are mean \pm SD, $n = 6$.

vehicle control (PBS), TF-011 (1 mg/kg), or TF-TCB at three different dose levels (0.2, 1 and 5 mg/kg) following Fig. 5A. Compared with PBS, TF-011 only exhibited moderate tumor growth inhibitory effect. While for all three doses of TF-TCB, significant tumor growth inhibition was observed from Day 7 to study completion with two mice in the TF-TCB group (dose of 0.2 mg/kg) having no detectable tumor at the end of the study ($P < 0.005$, Fig. 5B and C). The weight of tumors in the TF-TCB groups determined at the end of study was also remarkably lighter than that in the PBS group and TF-011 group ($P < 0.0001$, Fig. 5C). There was no obvious difference between TF-TCB groups with different doses, which was possible due to that the dose of TF-TCB was not low enough to reach the efficacy threshold ($P > 0.05$, Fig. 5B and C)⁴². Further study with lower TF-TCB dose will reveal the dose–response manner. Mice weight or other indicators of growth condition were not affected by any treatments throughout the study (Fig. 5B).

In order to study the mechanism of anti-tumor activity of TF-TCB in this model, tumors were stripped 6 days after first treatment (started four days after tumor inoculation) and IHC was performed. TF positive tumor cells in the tumors treated with TF-TCB were almost completely killed with low TF staining level observed (Fig. 5D and Supporting Information Table S5). There were almost no T cells (CD3 staining) in the tumors treated with PBS or TF-011, while in the tumors treated with TF-TCB, abundant T cells were observed (Fig. 5D and Supporting Information Table S6). These indicated that TF-TCB inhibited

tumor growth though induction of T cell proliferation and killing of TF⁺ tumor cells.

3.9. Tumor growth inhibition of TF-TCB in AsPC-1 xenograft model with intravenous transfer of PBMC

The *in vivo* efficacy of TF-TCB was further evaluated in AsPC-1 xenograft model with intravenous transfer of PBMC. In this model, PBMC were not co-grafted with tumor cells, and were required to be recruited from periphery to the tumor sites. Female NOG mice were firstly inoculated s.c. with AsPC-1 cells. Nine days later, tumor-bearing mice were distributed into four groups based on tumor volume ($n = 6$ /group) and transferred i.v. with 5×10^6 PBMC or PBS. The two groups receiving PBMC were then treated i.v. with PBS or TF-TCB (5 mg/kg), while other two groups were treated i.p. with PBS or gemcitabine (100 mg/kg) as the negative or positive control (Fig. 6A). Gemcitabine has been one of the effective chemotherapies in the clinic for treating pancreatic cancer⁴³. In some AsPC-1 xenograft models, anti-tumor effect of gemcitabine has also been illustrated^{44,45}. In this tumor model, tumor growth was noticeably delayed by gemcitabine at the early stage (ten days after first dose) ($P < 0.05$, Fig. 6B and C). However, its inhibitory activity weakened as tumor grew, with no significant tumor growth inhibitory effects at the end of the study ($P > 0.05$, Fig. 6B–D). Tumor growth was slightly inhibited by PBMC/PBS treatment throughout the study, while significant tumor growth inhibition was induced by PBMC/

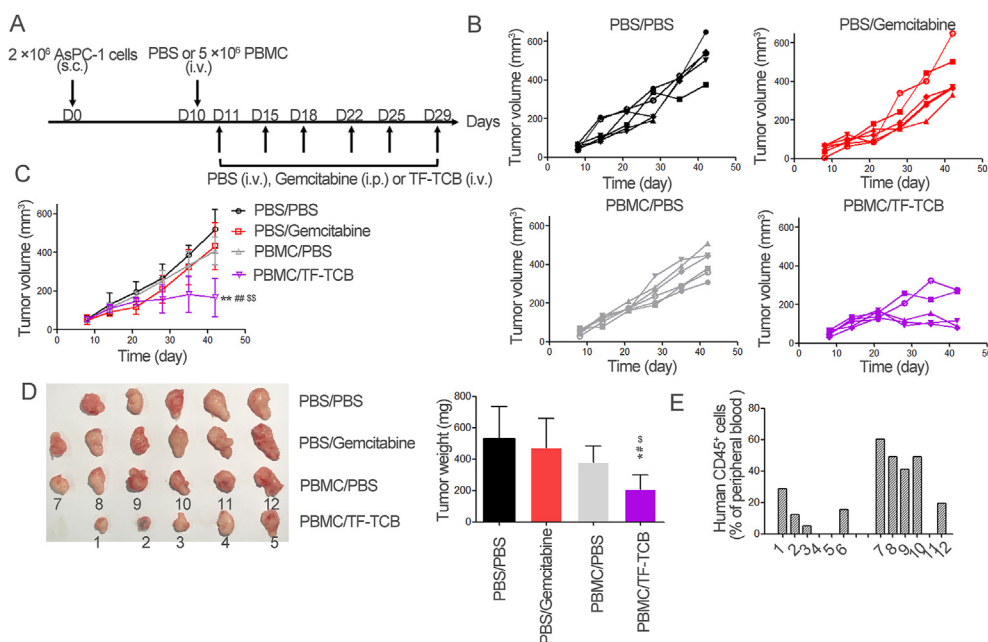


Figure 6 Inhibition of tumor growth by TF-TCB in AsPC-1 xenograft model with intravenous transfer of PBMC. (A) Schematic depiction of tumor inoculation and treatment protocol. Female NOG mice were implanted s.c. with 2×10^6 AsPC-1 cells on Day 0. On Day 9, mice were divided into four groups ($n = 6$ /group) based on tumor volume and 5×10^6 PBMC or PBS were injected i.v. into mice on Day 10. On Days 11–29, mice receiving PBMC were treated i.v. with PBS (PBMC/PBS group) and TF-TCB (5 mg/kg, PBMC/TF-TCB group), mice receiving PBS were treated intraperitoneally (i.p.) with PBS (PBS/PBS group) and gemcitabine (100 mg/kg, PBS/gemcitabine group). (B) Tumor volume of individual mice in each group measured throughout the study. (C) Tumor volume of the four groups. (D) Digital image and weight of the stripped tumors. There were only five tumors in the PBS/PBS and PBMC/TF-TCB group due to that one mouse in each group died before study ended. (E) Fourteen days after PBMC transfer, percentage of human CD45⁺ cells in peripheral blood of mice in PBMC/PBS and PBMC/TF-TCB group. 1–12 were mouse IDs, corresponding to tumor IDs in Fig. 6D. Statistical analysis was based on two-tailed heteroscedastic *t*-test. * $P < 0.05$ and ** $P < 0.01$ vs. PBS/PBS group; # $P < 0.05$ and ## $P < 0.01$ vs. PBMC/PBS group; \$ $P < 0.05$ and \$\$ $P < 0.01$ vs. PBS/gemcitabine group. Data are mean \pm SD, $n = 6$.

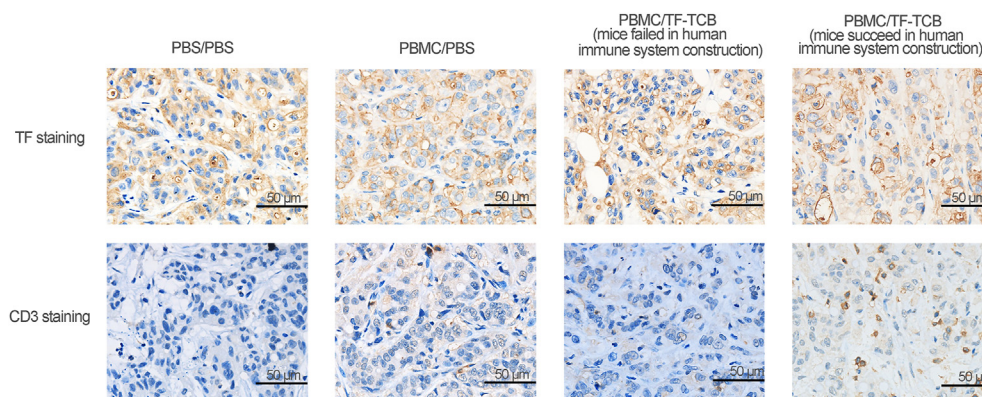


Figure 7 IHC analysis of stripped tumors in AsPC-1 xenograft model with intravenous transfer of PBMC. Tumors were stained for human TF and human CD3 (all brown) and were counterstained with hematoxylin (blue). Scale bar is indicated in each panel.

TF-TCB treatment since Day 28 ($P < 0.05$). The weight of tumors in PBMC/TF-TCB group was also remarkably lighter than that in other three groups ($P < 0.05$, Fig. 6D). Due to the incomplete immune system of this tumor model, more comparison between TF-TCB and Gemcitabine will be conducted in future study.

Fourteen days after PBMC engraftment, 4/6 mice in the PBMC/TF-TCB group and 5/6 mice in the PBMC/PBS group had succeeded in reconstruction of human immune system with detectable human CD45⁺ cells in peripheral blood (Fig. 6E). The

two mice (mice ID: 4 and 5) in the PBMC/TF-TCB group that had no detectable human CD45⁺ cells bore bigger tumor than other three mice, illustrating PBMC dependence of TF-TCB activity (Fig. 6D and E).

Tumors were collected at the end of the study and IHC was conducted. T cell infiltration into tumor was observed in mice bearing human immune system and receiving TF-TCB treatment (Fig. 7 and Supporting Information Table S7). The result confirmed the critical role of TF-TCB in tumor growth inhibition.

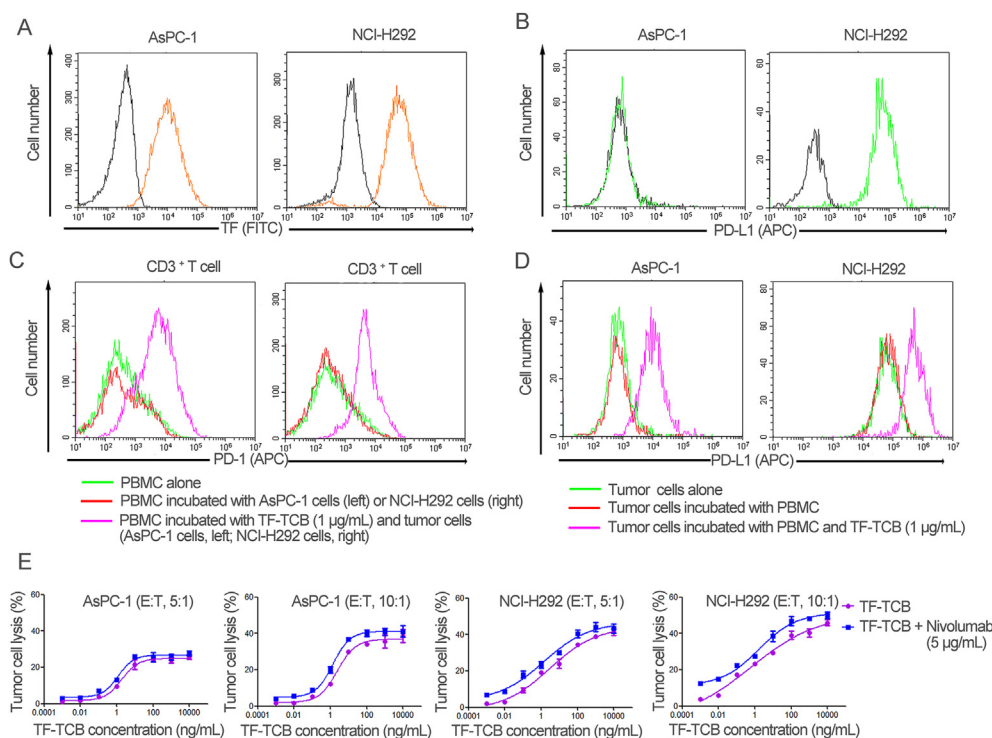


Figure 8 Efficacy of combination treatment of TF-TCB and nivolumab *in vitro*. (A) Relative TF expression on AsPC-1 and NCI-H292 cell lines, detected by flow cytometry. Orange histogram, tumor cells stained with FITC-labeled anti-TF antibody; black histogram, Blank Control. (B) Relative PD-L1 expression on AsPC-1 and NCI-H292 cell lines, detected by flow cytometry. Green histogram, tumor cells stained with APC-labeled anti-PD-L1 antibody; Black histogram, Blank Control. (C) PD-1 staining of CD3⁺ T cells after 36 h of incubation. (D) PD-L1 staining of AsPC-1 and NCI-H292 cells after 36 h of incubation. (E) Percentage of tumor cell lysis detected after 36 h of incubation of target cells (AsPC-1 and NCI-H292) with test antibodies and PBMC. Data are mean \pm SD, $n = 3$.

3.10. Combination treatment with anti-PD-1 antibody (nivolumab)

AsPC-1 and NCI-H292 are two TF⁺ tumor cell lines with different PD-L1 expression (Fig. 8A and B). It was revealed that PD-1 expression level on CD3⁺ T cells and PD-L1 expression level on AsPC-1 and NCI-H292 cells were elevated during TF-TCB-mediated tumor cell lysis (Fig. 8C and D). PD-1/PD-L1 interaction is an escape mechanism against T cell-based immunotherapy, whereas nivolumab is an anti-PD-1 antibody that can block PD-1/PD-L1 interaction and restore anti-tumor activity of T cells⁴⁶. To further improve the efficacy of TF-TCB, combination treatment of TF-TCB and nivolumab was evaluated *in vitro* and *in vivo*.

After 36 h of incubation of tumor cells (AsPC-1 or NCI-H292) with PBMC and test antibodies (TF-TCB, or combination of TF-TCB and nivolumab), cell lysis was measured (Fig. 8E). In spite of PD-L1 expressing in NCI-H292 cells, strong tumor cell lysis was achieved by TF-TCB. And for both AsPC-1 and NCI-H292 tumor cells, combination with nivolumab enhanced the anti-tumor activity of TF-TCB (by lowering TF-TCB dose to achieve the same percentage of tumor cell lysis) (Fig. 8E).

The efficacy of combination treatment of TF-TCB and nivolumab was further evaluated *in vivo* in NCI-H292 xenograft model with intravenous transfer of PBMC (Fig. 9A). Nivolumab has been approved by the US Food and Drug Administration for the treatment of several types of cancer, including lung cancer. However, it was only effective to tumors with enough T cell

infiltration^{37,47}. In this tumor model with poor T cell infiltration, no significant tumor growth inhibitory effect was achieved by nivolumab ($P > 0.05$, Fig. 9B and C). In contrast, tumor growth was prominently inhibited by both TF-TCB alone and combination treatment with nivolumab from Day 21 to study completion ($P < 0.005$). Additionally, combination treatment had a much better anti-tumor activity than TF-TCB alone, indicating that T cell activity was further enhanced by nivolumab ($P < 0.05$, Fig. 9B and C). Tumor weight determined at the end of the study also supported the remarkable tumor growth inhibitory activity of TF-TCB and combination therapy (Fig. 9D).

Fourteen days after PBMC engraftment, all mice had succeeded in reconstruction of human immune system with detectable human CD45⁺ cells in peripheral blood (Fig. 9E). In general, mice treated with TF-TCB had a lower percentage of human CD45⁺ cells than that treated with PBS. This may be due to that CD45⁺ cells especially CD3⁺ T cells were recruited to the tumor sites and needs further verification.

When study completed, tumors were retrieved and IHC was performed. In the tumor treated with TF-TCB + nivolumab and the center of tumor treated with TF-TCB, much lower percentage of TF⁺ cells was observed (Fig. 10 and Supporting Information Table S8). This indicated that TF⁺ tumor cells elimination was induced by TF-TCB treatment. The CD3 staining revealed that T cells were recruited into the tumors in both TF-TCB group and TF-TCB + nivolumab group (Fig. 10 and Supporting Information

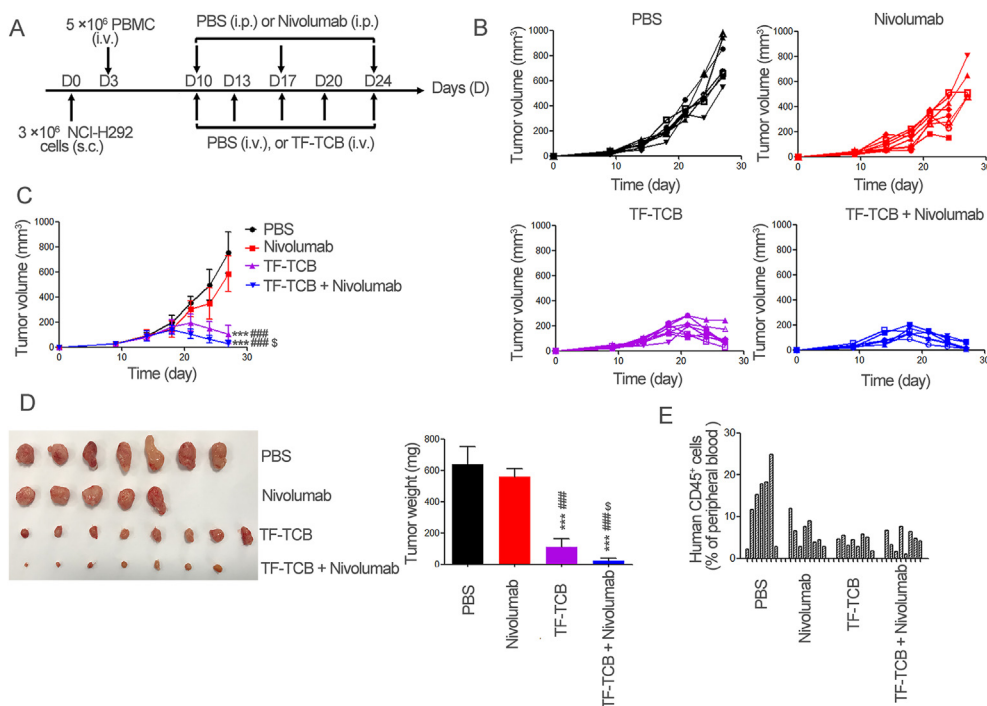


Figure 9 Efficacy of combination treatment of TF-TCB and nivolumab in NCI-H292 xenograft model with intravenous transfer of PBMC. (A) Schematic depiction of tumor inoculation and treatment protocol. Female NOG mice were implanted s.c. with 3×10^6 NCI-H292 cells on Day 0. On Day 3, 5×10^6 PBMC were injected i.v. into mice. On Days 9–24, mice were divided into four groups ($n = 8$ /group) based on tumor volume and treated with PBS (i.v.), TF-TCB (5 mg/kg, i.v.), nivolumab (10 mg/kg, i.p.) or combination of TF-TCB (5 mg/kg, i.v.) and nivolumab (10 mg/kg, i.p.). (B) Tumor volume of individual mice in each group measured throughout the study. (C) Tumor volume of four groups. (D) Digital image and weight of the stripped tumors (one mice in the PBS and TF-TCB + nivolumab group, three mice in the nivolumab group died before study ended). (E) Percentage of human CD45⁺ cells in mice peripheral blood 14 days after PBMC transfer. Statistical analysis was based on two-tailed heteroscedastic *t*-test. *** $P < 0.0001$ vs. PBS group; ### $P < 0.0001$ vs. Nivolumab group; \$ $P < 0.05$ vs. TF-TCB group. Data are mean \pm SD, $n = 8$.

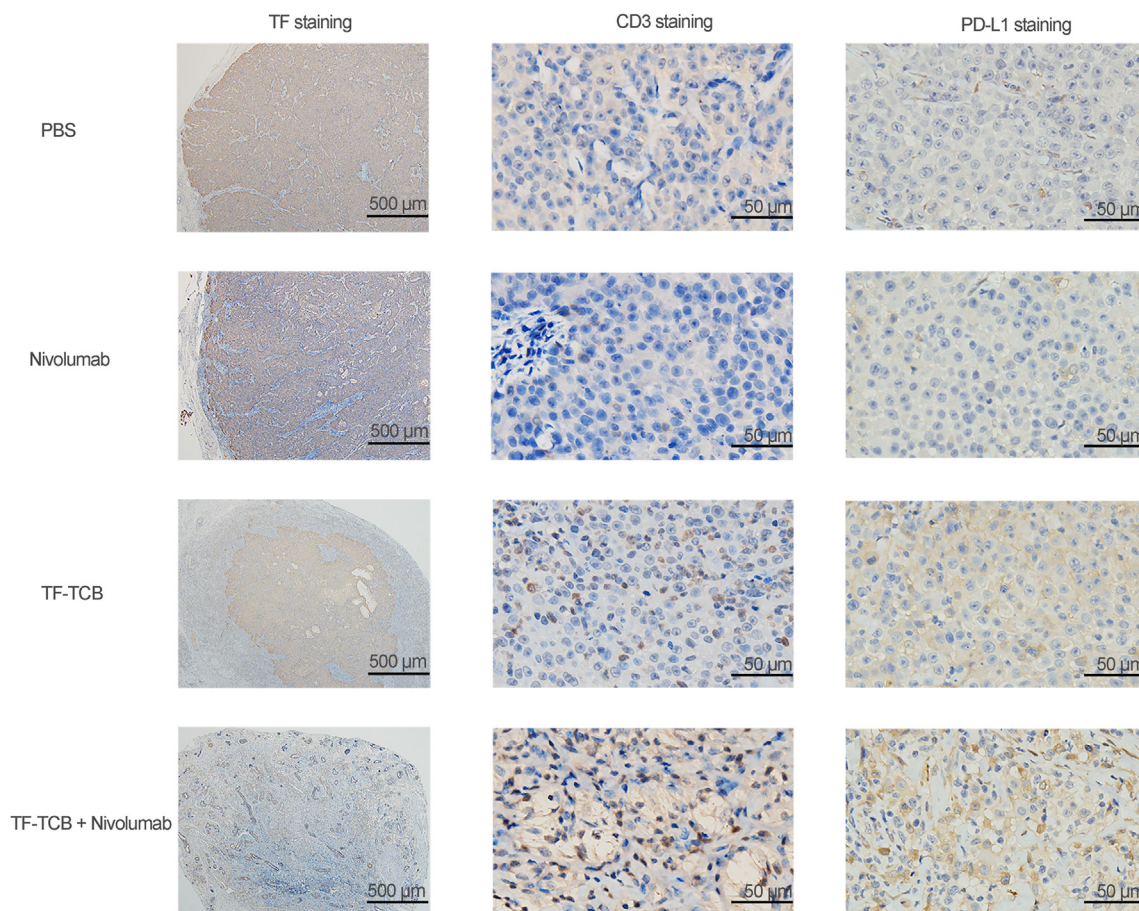


Figure 10 IHC analysis of stripped tumors in NCI-H292 xenograft model with intravenous transfer of PBMC. Tumors were stained for human TF, human CD3 and PD-L1 (all brown) and were counterstained with hematoxylin (blue). Scale bar is indicated in each panel.

Table S9). The higher H-Scores of PD-L1 staining of tumors in the TF-TCB group and TF-TCB + nivolumab group indicated that a more inflamed tumor microenvironment was induced by TF-TCB (Fig. 10 and Supporting Information Table S10).

4. Discussion

TCB is an efficacious immunotherapy for cancer treatment. Here we designed and characterized a novel TCB targeting TF (TF-TCB) to provide a potentially new direction to treat solid tumors.

TF was reported to be overexpressed in tumor tissues; however, most studies only focused on one carcinoma type and had no comparison with the normal tissues^{10–15,17,48}. In our study, TF expression was evaluated in five carcinoma types and normal tissues, which was an addition to the TF expression profile and provided basis for clinical studies. The overexpression of TF observed in all evaluated carcinoma types but not in most normal tissues made TF a specific ideal target for cancer treatment. Although TF expression was only found in limited normal cell types, toxicity of TF-TCB towards the normal tissues needs to be carefully evaluated in future studies.

IgG-[L]-scFv structure was adopted to produce TF-TCB in this study to avert the chain mis-pairing problems in bispecific antibody production^{34,56}. Our results demonstrate that the TF-TCB could be expressed and purified similar as a normal IgG1, providing the potential for large-scale production with good manufacturing practice.

The results from *in vitro* study show that TF-TCB was effective against a wide range of tumor cell lines regardless of PD-L1 expression and tumor type of the cell lines, indicating the potential of TF-TCB to treat broad spectrum of solid tumors. *In vivo*, a tumor cell/PBMC co-grafting model and two established tumor models with poor T cell infiltration were used to evaluate the efficacy of TF-TCB. Remarkably, strong tumor growth inhibition was induced by the TF-TCB in all models, indicating its promising prospect in solid tumors treatment.

Our results reveal the limited anti-tumor activity of immune-checkpoint inhibitors towards tumors with poor T cell infiltration. In contrast, strong activity of TF-TCB in the same circumstance was observed. Synergistic effect of combination of TF-TCB and immune-checkpoint inhibitors has been observed *in vitro* and *in vivo*, suggesting the TF-TCB mediated T cell activity was further unleashed by immune-checkpoint inhibitors, which was consistent with other TCBs^{49,50}. The sequencing of combinations and associated cytokine release syndrome should be evaluated in future studies. Besides immune-checkpoint inhibitors, T cell activation enhancer like CD28 antibody or OX40 antibody and anti-angiogenesis agents may also be explored to further improve the TF-TCB efficacy^{51,52}.

Up to now, there has been three TF-targeting cancer therapies in clinical trials (ALT-836, MORAb-066 and Tisotumab Vedotin). ALT-836 and MORAb-066 are two anti-TF antibodies and had no clinical progress since 2016. Tisotumab Vedotin is the only one

being tested in the clinical trials. Our results could potentially be an addition to the current approaches targeting TF. Although TF is a high turnover protein with rapid internalization, our results demonstrated that it could be targeted by TCB for cancer treatment. The internalization of TF was not a limiting factor for TF-TCB's activity in our experiments, which was in accordance with a report with CD33-TCB^{53,54}.

5. Conclusions

We have designed and characterized a novel TCB targeting TF-positive solid tumors. The TF-TCB showed powerful antitumor activity in multiple *in vitro* and *in vivo* models. It was efficacious in poorly T cell-infiltrated established tumors and had the ability to alter tumor microenvironment. In addition, anti-tumor activity of the TF-TCB was further enhanced by immune checkpoint blockade agents. Altogether, our results demonstrated the suitability of TF as a novel target for TCB and the effectiveness of the TF-TCB as a promising approach for solid tumors treatment.

Acknowledgments

This work was supported by the National Natural Science Foundation of China (Nos. 81773621 and 82073751) and the National Science and Technology Major Project (No. 2019ZX09201001, China). We are grateful to Yu Tang and Jingli Hou (Shanghai Jiao Tong University, Institute of Translational Medicine, Shanghai, China) for their assistance in Biacore-based affinity analysis. We thank the Haiyang Yin and Zongwei Hu (Shanghai Jiao Tong University, School of Pharmacy, Shanghai, China) for their help in animal study.

Author contributions

Jianwei Zhu, Xiaodong Xiao, Yueqing Xie, Hua Jiang and Zhidi Pan designed the experiment. Zhidi Pan, Jie Chen, Yuexian Zhou, Huifang Zong, Lei Wang and Rui Sun performed the experiments. Zhidi Pan analyzed and interpreted the data. Jianwei Zhu and Zhidi Pan wrote the manuscript. Jianwei Zhu, Xiaodong Xiao, Yueqing Xie, Hua Jiang, Baohong Zhang, Huili Lu, Yunsheng Yuan, Lei Han and Zhidi Pan contributed to manuscript editing. All authors read and approved the final manuscript.

Conflicts of interest

All authors declare no conflict of interest.

Appendix A. Supporting information

Supporting data to this article can be found online at <https://doi.org/10.1016/j.apsb.2021.10.028>.

References

- Labrijn AF, Janmaat ML, Reichert JM, Parren P. Bispecific antibodies: a mechanistic review of the pipeline. *Nat Rev Drug Discov* 2019;**18**:585–608.
- Kischel R, Hausmann S, Baeuerle P, Kufer P. Abstract #3252: effector memory T cells make a major contribution to redirected target cell lysis by T cell-engaging BiTE antibody MT110. *Cancer Res* 2009;**69**:3252.
- Choi BD, Gedeon PC, Herndon 2nd JE, Archer GE, Reap EA, Sanchez-Perez L, et al. Human regulatory T cells kill tumor cells through granzyme-dependent cytotoxicity upon retargeting with a bispecific antibody. *Cancer Immunol Res* 2013;**1**:163.
- Ishiguro T, Sano Y, Komatsu SI, Kamata-Sakurai M, Kaneko A, Kinoshita Y, et al. An anti-glypican 3/CD3 bispecific T cell-redirecting antibody for treatment of solid tumors. *Sci Transl Med* 2017;**9**:eaal4291.
- Bacac M, Fauti T, Sam J, Colombetti S, Weinzierl T, Ouaret D, et al. A novel carcinoembryonic antigen T-cell bispecific antibody (CEA TCB) for the treatment of solid tumors. *Clin Cancer Res* 2016;**22**:3286–97.
- Crawford A, Haber L, Kelly MP, Vazzana K, Canova L, Ram P, et al. A mucin 16 bispecific T cell-engaging antibody for the treatment of ovarian cancer. *Sci Transl Med* 2019;**11**:eaau7534.
- Topp MS, Gokbuget N, Stein AS, Zugmaier G, O'Brien S, Bargou RC, et al. Safety and activity of blinatumomab for adult patients with relapsed or refractory B-precursor acute lymphoblastic leukaemia: a multicentre, single-arm, phase 2 study. *Lancet Oncol* 2015;**16**:57–66.
- Yang J, Orloff MM, Sacco JJ, Hernandez-Aya LF, Lee K, Merrick S, et al. Resensitization of uveal melanoma (UM) to immune checkpoint inhibition (ICI) by IMCgp100 (IMC). *J Clin Oncol* 2019;**37**:9592.
- Van Dreden P, EpsilonIalamy I, Gerotziapas GT. The role of tissue factor in cancer-related hypercoagulability, tumor growth, angiogenesis and metastasis and future therapeutic strategies. *Crit Rev Oncog* 2017;**22**:219–48.
- Kaido T, Oe H, Yoshikawa A, Mori A, Arii S, Imamura M. Tissue factor is a useful prognostic factor of recurrence in hepatocellular carcinoma in 5-year survivors. *Hepatogastroenterology* 2005;**52**:1383–7.
- Seto S, Onodera H, Kaido T, Yoshikawa A, Ishigami S, Arii S, et al. Tissue factor expression in human colorectal carcinoma: correlation with hepatic metastasis and impact on prognosis. *Cancer* 2000;**88**:295–301.
- Ueno T, Toi M, Koike M, Nakamura S, Tominaga T. Tissue factor expression in breast cancer tissues: its correlation with prognosis and plasma concentration. *Br J Cancer* 2000;**83**:164–70.
- Akashi T, Furuya Y, Ohta S, Fuse H. Tissue factor expression and prognosis in patients with metastatic prostate cancer. *Urology* 2003;**62**:1078–82.
- Patry G, Hovington H, Larue H, Harel F, Fradet Y, Lacombe L. Tissue factor expression correlates with disease-specific survival in patients with node-negative muscle-invasive bladder cancer. *Int J Cancer* 2008;**122**:1592–7.
- Chen LJ, Luo GH, Tan Y, Wei J, Wu C, Zheng L, et al. Immunolocalisation of tissue factor in esophageal cancer is correlated with intratumoral angiogenesis and prognosis of the patient. *Acta Histochem* 2010;**112**:233–9.
- Kakkar AK, Lemoine NR, Scully MF, Tebbutt S, Williamson RC. Tissue factor expression correlates with histological grade in human pancreatic cancer. *Br J Surg* 1995;**82**:1101–4.
- Hisada Y, Mackman N. Tissue factor and cancer: regulation, tumor growth, and metastasis. *Semin Thromb Hemost* 2019;**45**:385–95.
- Drake TA, Morrissey JH, Edgington TS. Selective cellular expression of tissue factor in human tissues. Implications for disorders of hemostasis and thrombosis. *Am J Pathol* 1989;**134**:1087–97.
- Gessler F, Voss V, Dutzmann S, Seifert V, Gerlach R, Kogel D. Inhibition of tissue factor/protease-activated receptor-2 signaling limits proliferation, migration and invasion of malignant glioma cells. *Neuroscience* 2010;**165**:1312–22.
- Versteeg HH, Schaffner F, Kerver M, Petersen HH, Ahamed J, Felding-Habermann B, et al. Inhibition of tissue factor signaling suppresses tumor growth. *Blood* 2008;**111**:190–9.

21. Breij EC, de Goeij BE, Verploegen S, Schuurhuis DH, Amirkhosravi A, Francis J, et al. An antibody–drug conjugate that targets tissue factor exhibits potent therapeutic activity against a broad range of solid tumors. *Cancer Res* 2014;**74**:1214–26.
22. de Bono JS, Concin N, Hong DS, Thistlethwaite FC, Machiels JP, Arkenau HT, et al. Tisotumab vedotin in patients with advanced or metastatic solid tumours (InnovaTV 201): a first-in-human, multi-centre, phase 1–2 trial. *Lancet Oncol* 2019;**20**:383–93.
23. Hong DS, Concin N, Vergote I, de Bono JS, Slomovitz BM, Drew Y, et al. Tisotumab vedotin in previously treated recurrent or metastatic cervical cancer. *Clin Cancer Res* 2020;**26**:1220–8.
24. Portolano N, Watson PJ, Fairall L, Millard CJ, Milano CP, Song Y, et al. Recombinant protein expression for structural biology in HEK 293F suspension cells: a novel and accessible approach. *J Vis Exp* 2014:e51897.
25. Han L, Chen JS, Ding K, Zong HF, Xie YQ, Jiang H, et al. Efficient generation of bispecific IgG antibodies by split intein mediated protein trans-splicing system. *Sci Rep* 2017;**7**:8360.
26. Oberst MD, Fuhrmann S, Mulgrew K, Amann M, Cheng L, Lutterbuese P, et al. CEA/CD3 bispecific antibody MEDI-565/AMG 211 activation of T cells and subsequent killing of human tumors is independent of mutations commonly found in colorectal adenocarcinomas. *MAbs* 2014;**6**:1571–84.
27. Manikwar P, Mulagapati SHR, Kasturirangan S, Moez K, Rainey GJ, Lobo B. Characterization of a novel bispecific antibody with improved conformational and chemical stability. *J Pharm Sci* 2020;**109**:220–32.
28. Zhou YX, Zong HF, Han L, Xie YQ, Jiang H, Gilly J, et al. A novel bispecific antibody targeting CD3 and prolactin receptor (PRLR) against PRLR-expression breast cancer. *J Exp Clin Cancer Res* 2020;**39**:87.
29. Toneto MG, Depaula PL, Debon L, Tertuliano B, Silva VD, Baldissero M, et al. Immunohistochemical analysis of tissue factor expression in gastric carcinoma: correlations with prognosis and survival. *Rev Col Bras Cir* 2018;**45**:e2030.
30. Lo L, Valentine H, Harrison J, Hayes S, Welch I, Pritchard S, et al. Tissue factor expression in the metaplasia–adenoma–carcinoma sequence of gastric cancer in a European population. *Br J Cancer* 2012;**107**:1125–30.
31. Kaushal V, Mukunyadzi P, Siegel ER, Dennis RA, Johnson DE, Kohli M. Expression of tissue factor in prostate cancer correlates with malignant phenotype. *Appl Immunohistochem Mol Morphol* 2008;**16**:1–6.
32. Adair JR, Athwal DS, Bodmer MW, Bright SM, Collins AM, Pulito VL, et al. Humanization of the murine anti-human CD3 monoclonal antibody OKT3. *Hum Antibodies Hybridomas* 1994;**5**:41–7.
33. Concin N, Vergote IB, Lassen UN, Drew Y, Machiels JP, Arkenau HT, et al. A phase IIa study of tisotumab vedotin in patients with previously treated recurrent or metastatic cervical cancer: updated analysis of full cervical expansion cohort. *Ann Oncol* 2018;**29**:344.
34. Santich BH, Park JA, Tran H, Guo HF, Huse M, Cheung NV. Inter-domain spacing and spatial configuration drive the potency of IgG-[L]-scFv T cell bispecific antibodies. *Sci Transl Med* 2020;**12**:eaax1315.
35. Orcutt KD, Ackerman ME, Cieslewicz M, Quiroz E, Slusarczyk AL, Frangioni JV, et al. A modular IgG-scFv bispecific antibody topology. *Protein Eng Des Sel* 2010;**23**:221–8.
36. Schlothauer T, Herter S, Koller CF, Grau-Richards S, Steinhart V, Spick C, et al. Novel human IgG1 and IgG4 Fc-engineered antibodies with completely abolished immune effector functions. *Protein Eng Des Sel* 2016;**29**:457–66.
37. Hamanishi J, Mandai M, Ikeda T, Minami M, Kawaguchi A, Murayama T, et al. Safety and antitumor activity of anti-PD-1 antibody, nivolumab, in patients with platinum-resistant ovarian cancer. *J Clin Oncol* 2015;**33**:4015–22.
38. Ionescu RM, Vlasak J, Price C, Kirchmeier M. Contribution of variable domains to the stability of humanized IgG1 monoclonal antibodies. *J Pharm Sci* 2008;**97**:1414–26.
39. Chennamsetty N, Voynov V, Kayser V, Helk B, Trout BL. Design of therapeutic proteins with enhanced stability. *Proc Natl Acad Sci U S A* 2009;**106**:11937–42.
40. Lopez-Albaitero A, Xu H, Guo HF, Wang LL, Wu ZH, Tran H, et al. Overcoming resistance to HER2-targeted therapy with a novel HER2/CD3 bispecific antibody. *OncImmunology* 2017;**6**:e1267891.
41. Xu H, Cheng M, Guo HF, Chen YD, Huse M, Cheung NK. Retargeting T cells to GD2 pentasaccharide on human tumors using bispecific humanized antibody. *Cancer Immunol Res* 2015;**3**:266–77.
42. Zuch de Zafra CL, Fajardo F, Zhong W, Bennett MJ, Muchhal US, Moore GL, et al. Targeting multiple myeloma with AMG 424, a novel anti-CD38/CD3 bispecific T-cell-recruiting antibody optimized for cytotoxicity and cytokine release. *Clin Cancer Res* 2019;**25**:3921–33.
43. Kamisawa T, Wood LD, Itoi T, Takaori K. Pancreatic cancer. *Lancet* 2016;**388**:73–85.
44. Jung DB, Yun MY, Kim EO, Kim J, Kim B, Jung JH, et al. The heparan sulfate mimetic PG545 interferes with Wnt/ β -catenin signaling and significantly suppresses pancreatic tumorigenesis alone and in combination with gemcitabine. *Oncotarget* 2015;**6**:4992–5004.
45. Huang HL, Chao MW, Chen CC, Cheng CC, Chen MC, Lin CF, et al. LTP-1, a novel antimitotic agent and Stat3 inhibitor, inhibits human pancreatic carcinomas *in vitro* and *in vivo*. *Sci Rep* 2016;**6**:27794.
46. Alsaab HO, Sau S, Alzhrani R, Tatiparti K, Bhise K, Kashaw SK, et al. PD-1 and PD-L1 checkpoint signaling inhibition for cancer immunotherapy: mechanism, combinations, and clinical outcome. *Front Pharmacol* 2017;**8**:561.
47. Motzer RJ, Escudier B, McDermott DF, George S, Hammers HJ, Srinivas S, et al. Nivolumab *versus* everolimus in advanced renal-cell carcinoma. *N Engl J Med* 2015;**373**:1803–13.
48. Rondin AMR, Kroone C, Kapteijn MY, Versteeg HH, Buijs JT. Role of tissue factor in tumor progression and cancer-associated thrombosis. *Semin Thromb Hemost* 2019;**45**:396–412.
49. Chang CH, Wang Y, Li RX, Rossi DL, Liu DL, Rossi EA, et al. Combination therapy with bispecific antibodies and PD-1 blockade enhances the antitumor potency of T cells. *Cancer Res* 2017;**77**:5384–94.
50. Junntila TT, Li J, Johnston J, Hristopoulos M, Clark R, Ellerman D, et al. Antitumor efficacy of a bispecific antibody that targets HER2 and activates T cells. *Cancer Res* 2014;**74**:5561–71.
51. Skokos D, Waite JC, Haber L, Crawford A, Hermann A, Ullman E, et al. A class of costimulatory CD28-bispecific antibodies that enhance the antitumor activity of CD3-bispecific antibodies. *Sci Transl Med* 2020;**12**:eaaw7888.
52. Chiu D, Tavare R, Haber L, Aina OH, Vazzana K, Ram P, et al. A PSMA-targeting CD3 bispecific antibody induces antitumor responses that are enhanced by 4-1BB costimulation. *Cancer Immunol Res* 2020;**8**:596–608.
53. de Goeij BE, Satijn D, Freitag CM, Wubbolts R, Bleeker WK, Khasanov A, et al. High turnover of tissue factor enables efficient intracellular delivery of antibody–drug conjugates. *Mol Cancer Ther* 2015;**14**:1130–40.
54. Hoseini SS, Guo HF, Wu ZH, Hatano MN, Cheung NV. A potent tetravalent T-cell-engaging bispecific antibody against CD33 in acute myeloid leukemia. *Blood Adv* 2018;**2**:1250–8.
55. Sun R, Zhou YX, Han L, Pan ZD, Chen J, Zong HF, et al. A rational designed novel bispecific antibody for the treatment of GBM. *Biomedicines* 2021;**9**:640.
56. Chen J, Pan ZD, Han L, Zhou YX, Zong HF, Wang L, et al. A novel bispecific antibody targeting CD3 and Lewis Y with potent therapeutic efficacy against gastric cancer. *Biomedicines* 2021;**9**:1059.